Science of the Total Environment 760 (2021) 143935

Contents lists available at ScienceDirect

Science of the Total Environment

journal homepage: www.elsevier.com/locate/scitotenv

Isotopic source analysis of nitrogen-containing aerosol: A study of $PM_{2.5}$ in Guiyang (SW, China)

Jing Tian [a,b], Hui Guan [a], Yunhong Zhou [a,b], Nengjian Zheng [c], Hongwei Xiao [c], Jingjing Zhao [a,b], Zhongyi Zhang [a,b,c], Huayun Xiao [a,d,*]

[a] State Key Laboratory of Environmental Geochemistry, Institute of Geochemistry, Chinese Academy of Sciences, Guiyang 550081, China
[b] University of Chinese Academy of Sciences, Beijing 100049, China
[c] Key Laboratory of the Causes and Control of Atmospheric Pollution, East China University of Technology, Nanchang 330000, China
[d] School of Environmental Science and Engineering, Shanghai Jiao Tong University, Shanghai 200000, China

HIGHLIGHTS

- Nitrogen isotopes in PM2.5 were characterized in Guiyang.
- Seven source factors were identified for PM2.5 using the SIAR model.
- Source of biomass burning played a pivotal role in $PM_{2.5}$ during winter.

GRAPHICAL ABSTRACT

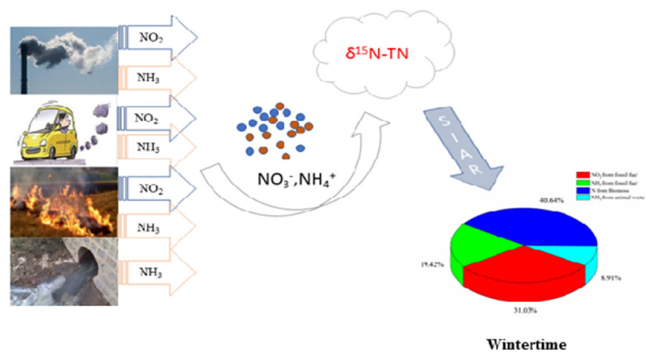

ARTICLE INFO

Article history:
Received 20 August 2020
Received in revised form 15 November 2020
Accepted 16 November 2020
Available online 5 December 2020

Editor: Pingqing Fu

Keywords:
$PM_{2.5}$
Nitrogen
δ^{15}N-TN
Winter sources
Biomass burning

ABSTRACT

The source of fine particulate matter ($PM_{2.5}$) has been a longstanding subject of debate, the nitrogen-15 isotope ($\delta^{15}N$) has been used to identify the major sources of atmospheric nitrogen. In this study, $PM_{2.5}$ samples ($n = 361$) were collected from September 2017 to August 2018 in the urban area of Guiyang (SW, China), to investigate the chemical composition and potential sources of $PM_{2.5}$. The results showed an average $PM_{2.5}$ of 33.0 μg m^{-3} ± 20.0 μg m^{-3}. The concentration of $PM_{2.5}$ was higher in Winter, lower in Summer. The major water resolved inorganic ions (WSIIs) were Ca^{2+}, NH_4^+, Na^+, SO_4^{2-}, NO_3^-, Cl^-. Nitrogen-containing aerosols (i.e., NO_3^- and NH_4^+) suddenly strengthened during the winter, when NO_3^- became the dominant contributor. Over the sampling period, the molar ratio of $NH_4^+/(NO_3^- + 2 \times SO_4^{2-})$ ranged from 0.1 to 0.9, thus indicating the full fixation of NH_4^+ by existing NO_3^- and SO_4^{2-} in $PM_{2.5}$. The annual value of NOR was 0.1 while rised to 0.5 in Winter. The variations of NOR (Nitrogen oxidation ratio) (0.1–0.5) values suggest that the secondary formation of NO_3^- occurred every season and was most influential during the winter. The total particulate nitrogen (TN) $\delta^{15}N$ value of $PM_{2.5}$ ranged from −5.9‰ to 25.3‰ over the year with annual mean of +11.8‰ ± 4.7‰, whereas it was between −5.9‰ and 14.3‰ during the winter with mean of 7.0‰ ± 3.8‰. A Bayesian isotope mixing model (Stable Isotope Analysis in R; SIAR) was applied to analyze the nitrogen sources. The modeling results showed that 29%, 21%, and 40% of TN in $PM_{2.5}$ during the winter in Guiyang was due to nitrogen-emissions from coal combustion, vehicle exhausts, and biomass burning, respectively. Our results demonstrate that biomass burning was the main contributor to PM during the winter, 80% of the air mass comes from rural areas of Guizhou border, this transport process can increase the risk of particulate pollution in Guiyang.

* Corresponding author at: State Key Laboratory of Environmental Geochemistry, Institute of Geochemistry, Chinese Academy of Sciences, Guiyang 550081, China.
E-mail address: xiaohuayun@vip.gyig.ac.cn (H. Xiao).

https://doi.org/10.1016/j.scitotenv.2020.143935
0048-9697/

1. Introduction

Aerosols have a strong influence on critical processes in the atmosphere that are related to air quality, climate change, visibility, and rainfall (Fuzzi et al., 2015), these meteorological factors can cause ecological and environmental problems. Moreover, air particulate matter with a particle diameter of ≤2.5 ($PM_{2.5}$) has adverse effects on human health (Pope et al., 2009; WHO, 2018).

China is experiencing a severe problem of particulate pollution due to the increased consumption of fossil fuels. Despite years of government efforts to reduce anthropogenic emissions, PM smog incidents still occur frequently, especially in some industrial and urban areas (e.g., Beijing, Shanghai) (Cheng et al., 2017; Tan et al., 2018). Previous studies have shown that the formation of PM haze is caused by high concentration of gas precursors (such as NOx and SO_2) and stagnation conditions (weak wind speed and high relative humidity) (Petäjä et al., 2016; Xu et al., 2017a; Zhang et al., 2009). Total particulate nitrogen (TN) mainly exists in the atmosphere in the form of NH_4^+-N and NO_3^--N, which are the main components of secondary inorganic aerosols. Previous studies found that the abundance of N in water-soluble inorganic ions (WSIIs) in polluted air ranged from 14% to 66% (Jiang et al., 2018; Liang et al., 2017; Tao et al., 2018). In recent years, with the sharp reduction of SO_2 emissions and the rapid increase of vehicle exhaust emissions, $PM_{2.5}$ in China has shifted from SO_4^{2-}-based PM to NO_3^--based PM (Pan et al., 2016). Previous studies have shown that NO_X emission sources is responsible for the change of $^{15}N(NO_3^-)$, and the exact mechanism of its rapid increase has not been well explained, which is mainly related to the change of 15 $N(NO_3^-)$ (He et al., 2018; He et al., 2020). In other words, N-containing aerosols have become a significant source of $PM_{2.5,}$ especially during haze events (Li et al., 2017; Xu et al., 2017b). Therefore, the estimation of the sources of TN can provide information for controlling the emission of N-containing aerosol and reducing the level of PM. Stable isotopes of N (e.g., $\delta^{15}N$) have been used to trace relevant sources and processes of atmospheric N(Heaton, 1986; Kendall et al., 2008; Michalski et al., 2004; Pavuluri et al., 2010; Savarino et al., 2013). The analysis of the $\delta^{15}N$ value in $PM_{2.5}$ is a relatively quick method compared to the $\delta^{15}N$ measurements of inorganic ($\delta^{15}N$-NO_3^- and $\delta^{15}N$-NH_4^+) and organic N components (Bikkina et al., 2016; Hegde et al., 2016; Widory, 2007) and also provides valuable information regarding the $\delta^{15}N$ value of N deposition (Yeatman et al., 2001a; Zhao et al., 2019).

Guiyang is the capital city of Guizhou Province. It is the first national forest city, one of the central industrial cities in southwest China, and is also famous for its good ecological environment and vacation tourism. It has a subtropical humid and temperate climate with an annual mean temperature of 15.3 °C and a mean annual relative humidity of 77%. Guiyang has experienced severe acid rain for a long time due to its extensive use of coal (Xiao and Liu, 2002). Although the situation improved somewhat following the strict control of coal use, the rapid increase in car use and industry are associated with an estimated annual emission of 20.2 kt yr^{-1} of NO_x. The total annual emission of NO_x-N in Guiyang during 2010 was 36.6 kg N ha^{-1} yr^{-1} (Xu et al., 2017c). Hence, Guiyang faces the challenge of N pollution in aerosols. In this work, daily $PM_{2.5}$ samples were collected in Guiyang between September 2017 and August 2018, and the $WSII_S$ concentrations, TN concentration, and $\delta^{15}N$ value were determined seasonally and annually in order to provide some insights into the wintertime $\delta^{15}N$-TN.

2. Methods

2.1. Sample collection

A total of 361 aerosol samples were collected in Guiyang between September 2017 and August 2018. The sampling site is located at the Institute of Geochemistry, Chinese Academy of Sciences (26.350° N, 106.430° E) (Fig. 1), and is a typical urban site of Guiyang. Aerosol samples of $PM_{2.5}$ were collected using quartz filters (8 × 10 in., Tissuquartz™ Filters, 2500 QAT-UP, Pallflex, Washington, USA) and a KC-1000 sampler (LaoShan Institute for Electronic Equipment, Qingdao, China) at a high flow rate of (1.05 ± 0.03) m^3 min^{-1}. The sampling time started at 18:00 and lasted for 23.5 h. Daily samples were collected and immediately stored in a refrigerator at −20 °C awaiting analysis (Zhang et al., 2020a).

2.2. Ion analysis

The quartz filter samples were further analyzed using ion chromatography (IC) (Dionex ICS-1100 and ICS-900; Thermo Scientific, USA). The samples were extracted using ultrapure water (Millipore, 18.2 MΩ) for 0.5 h in an ultrasonic bath, and were then centrifuged at 4200 r min^{-1} for 10 min using a shaker at room temperature(22 °C) (Zhang et al., 2020b). Each sample solution was filtered twice through

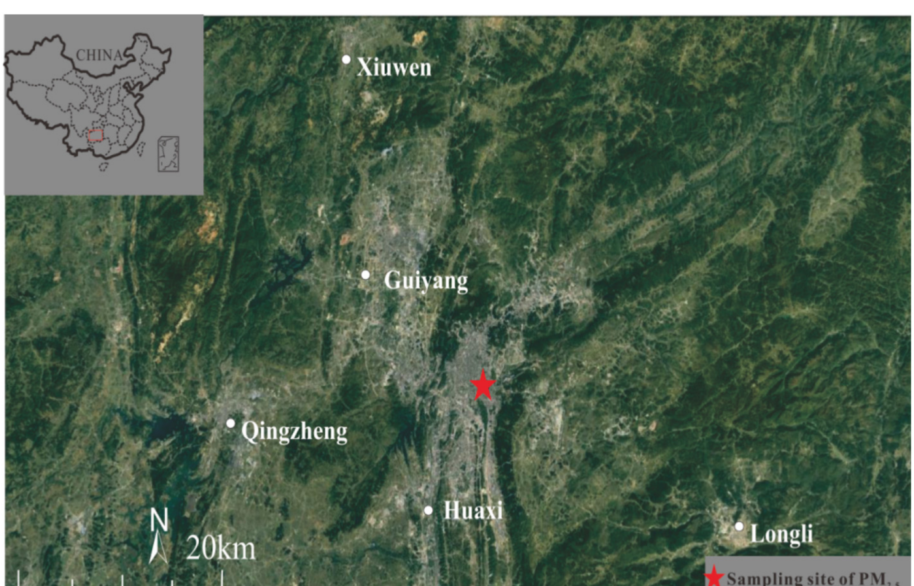

Fig. 1. Location of the sampling site in this study.

a Millipore syringe filter with a porosity of 0.22 μm. The major WSIIs (cations: Na^+, NH_4^+, K^+, Mg^{2+}, and Ca^{2+}; anions: F^-, Cl^-, NO_3^-, and SO_4^{2-}) in each extract were analyzed using IC (Dionex ICS-1100 for anions and Dionex ICS-900 for cations). Anions were analyzed using a self-regenerating anion suppressor (ASRS 300) and an AS11-HC analytical column with a Dionex conductivity detector. Cations were analyzed using a self-regenerating cation suppressor (CSRS-300) and a CG12A analytical column with a Dionex conductivity detector. The precision for all ionic species was >5%. The method detection limits were $0.0051 * 10^{-3}$ μg ml^{-1} for Cl^-, $0.0216 * 10^{-3}$ μg ml^{-1} for NO_3^-, $0.0115 * 10^{-3}$ μg ml^{-1} for SO_4^{2-}, $0.001 * 10^{-3}$ μg ml^{-1} for Na^+, $1.21 * 10^{-3}$ μg ml^{-1} for NH_4^+, $1.77 * 10^{-3}$ μg ml^{-1} for K^+, $2.47 * 10^{-3}$ μg ml^{-1} for Mg^{2+}, and $0.09 * 10^{-3}$ μg ml^{-1} for Ca^{2+} (Zhang et al., 2020c).

2.3. Isotope analysis

For the measurements of the TN stable isotope ratios, small filter discs (area of 0.5 cm^2, 1.13 cm^2, or 2.01 cm^2) were placed one at a time into a precleaned tin cup that was shaped into a small marble crucible using a pair of tweezers, and was introduced into the elemental analyzer (EA; Flash 2000) using an autosampler. Inside the EA, samples were first oxidized in a quartz column heated to 960 °C, the tin/marble was heated to oxidize all of the carbon and nitrogen species to CO_2 and nitrogen oxides, which then reduced to N_2. Subsequently, CO_2 and N_2 were separated on a gas chromatographic column, which was installed in the EA, and were measured with a thermal conductivity detector for TN. The samples were then transferred into an EA isotope-ratio mass spectrometer (EA–IRMS; MAT253 Plus, Thermo Fisher Scientific) through a Conflo IV interface to monitor the $^{15}N/^{14}N$ ratio. An acetanilide external standard (from Thermo Electron Corp.) was used to determine the calibration curves before every set of measurements for calculating the TN isotope values. The $\delta^{15}N$ values of the acetanilide standard were USGS41a (+37.626‰) and IAEA-N-2 (+20.3‰). The average standard deviation of the repeated analysis of the $\delta^{15}N$ value for an individual sample was ±0.2‰. The $\delta^{15}N$ value was calculated using Eq. (1) and is expressed in parts per mil (‰):

$$\delta^{15}N\ (‰) = \left[\left({}^{15}N/{}^{14}N\right)_{Sample}/\left({}^{15}N/{}^{14}N\right)_{Standard} - 1\right] \times 1000 \quad (1)$$

The isotope ratios were expressed in per mil (‰) relative to atmospheric N_2, standard = N_2 in air ($^{15}N/^{14}N = 0.00368$).

2.4. Meteorology and gas data

The ambient temperature (T, °C) and relative humidity (RH, %) data were provided by the China Meteorological Data Network of the National Meteorological Administration (http://www.cma.gov.cn/). Gas pollutant data (NO_2, SO_2, CO, and O_3) was also obtained from National Urban Air 126 Quality Real-Time Publishing Platform (http://106.37.208.233:20035/)..

2.5. Bayesian isotope mixing model

The proportional contributions (F, %) of significant sources to N in $PM_{2.5}$ were estimated using the Stable Isotope Analysis in R (SIAR) model. This model uses a Bayesian framework to establish a logical prior distribution based on the Dirichlet distribution (Evans et al., 2000), and then determines the probability distribution for the contribution of each source to the mixture(Jackson et al., 2009; Parnell et al., 2010). The model can substantially incorporate the uncertainties associated with multiple sources, fractionations, and isotope signatures (Moore and Semmens, 2008). In our estimations, the uncertainties should be evaluated for the $\delta^{15}N$ variability of TN in both $PM_{2.5}$ and N sources, and the isotopic effect of NH_3 (g) ↔ NH_4^+ (p) equilibrium.

The mixing model(Parnell et al., 2010) can be expressed by defining a set of N-mixture measurements for J isotope by K source contributors, as follows:

$$X_{ij} = \sum_{k=1}^{k} F_k \left(s_{jk} + c_{jk}\right) + \varepsilon_{ij} \quad (2)$$

$$s_{jk} \sim N\left(\mu_{jk}, \omega_{jk}^2\right)$$

$$c_{jk} \sim N\left(\lambda_{jk}, \tau_{jk}^2\right)$$

$$\varepsilon_{ij} \sim N\left(0, \sigma_j^2\right)$$

where all F values sum to unity; X_{ij} is the isotope value j of the mixture i, in which $i = 1, 2, 3, \ldots, N$ and $j = 1, 2, 3, \ldots, J$; S_{jk} is the source value k for isotope j ($k = 1, 2, 3, \ldots, K$), and is normally distributed with a mean μ_{jk} and standard deviation ω_{jk}. F_k is the proportion of source k estimated by the SIAR model; c_{jk} is the fractionation factor for isotope j on source k and is normally distributed with a mean λ_{jk} and standard deviation τ_{jk}. ε_{jk} is the residual error representing the additional unquantified variation between individual mixtures, and is normally distributed with a mean of 0 and a standard deviation σ_j, as described in detail elsewhere.(Jackson et al., 2009; Moore and Semmens, 2008; Parnell et al., 2010) To estimate the contributions of different N sources to the $PM_{2.5}$ in the winter samples ($n = 90$), one isotope ($j = 1$) ($\delta^{15}N$ of TN) and seven potential N-sources (Table 1) were used. The $\delta^{15}N$ variations of seven dominant N-sources in the urban center (NO_x from vehicle exhausts, coal combustion, and biomass burning; NH_3 from coal combustion, vehicle exhausts, animal waste, and biomass burning) (Wang et al., n.d.) were reported in previous studies (Table 1).

2.6. 2.6 Backward trajectories

Using the Geographic Information System (GIS) application MeteoinfoMap and the Global Data Assimilation System (GDAS), a 3 d (72 h) back-trajectory analysis was conducted to trace the source area of air masses arriving in Guiyang (up to an altitude of 1000 m above the sampling point). Fig. 2 showed the air mass back-trajectories for Guiyang from September 2017 to August 2018 as classified by the clustering method.

Table 1
Compiled $\delta^{15}N$ values (mean ± SD) of major NO_x and NH_3 emissions from different sources.

Source	N species	$\delta^{15}N$ (‰)	Reference
Coal combustion	NO_x	+19.8 ± 5.2	(Felix et al., 2012)
Vehicle exhausts	NO_x	−2.5 ± 1.5	(Walters et al., 2015)
Biomass burning	NO_x	+12.5 ± 3.1	(Hastings et al., 2009); (Felix et al., 2012)
Coal combustion	NH_3	−8.9 ± 4.1	(Felix et al., 2013)
Vehicle exhausts	NH_3	−3.4 ± 1.7	(Felix et al., 2013)
Biomass burning	NH_3	+12.0 ± na	(Kawashima and Kurahashi, 2011)
Animal waste	NH_3	−19.0 ± 14.1	(Freyer, 1978); (Heaton, 1987); (Felix et al., 2014), (Felix et al., 2013)

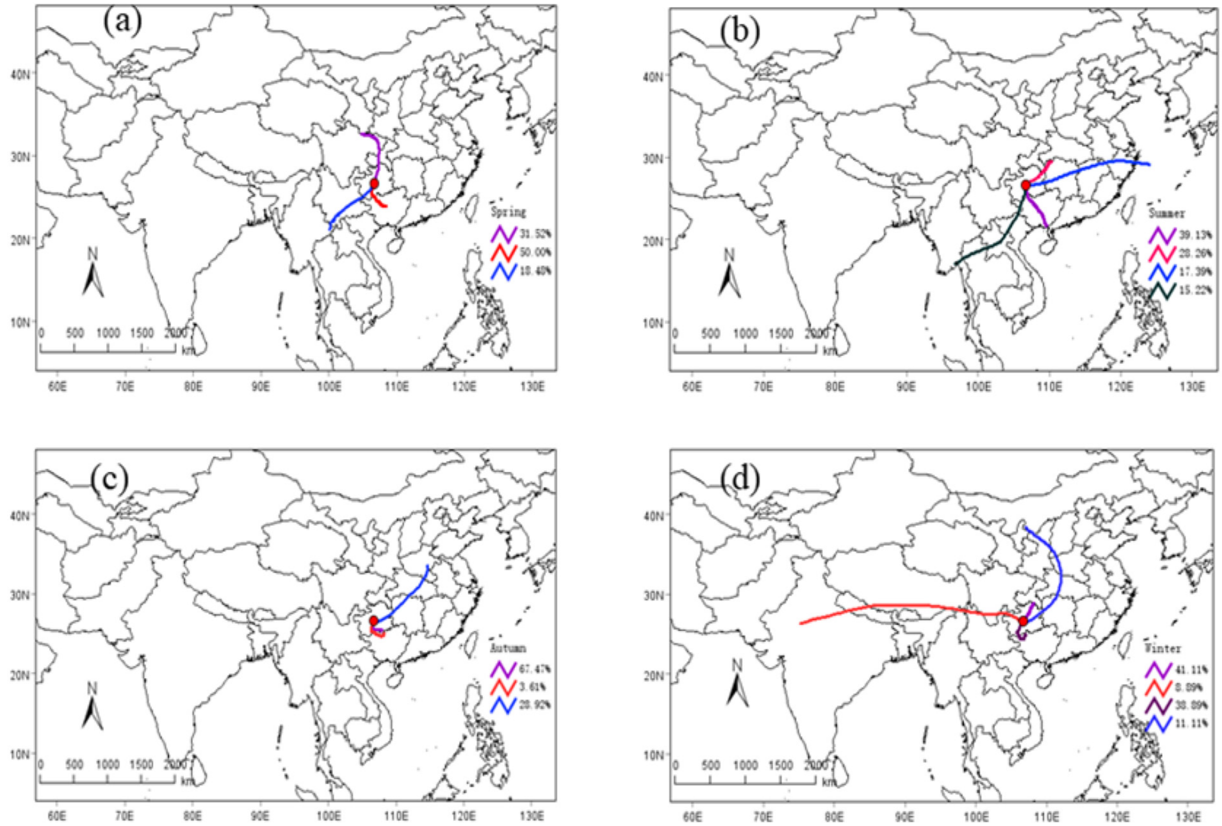

Fig. 2. Back-trajectory clustering results for 2017.9– 2018.8 at Guiyang. a, b, c, d represent Spring, summer, autumn, and Winter respectively(different color showed the trajectories and the proportion of air masses expressed as a percentage).

3. Result and discussion

3.1. Chemical characteristics of $PM_{2.5}$

Table 2 lists the seasonal and annual mean $PM_{2.5}$ mass concentrations, the mean concentrations of chemical constituents of $PM_{2.5}$, and the mean concentrations gaseous pollutants determined from the samples. The $PM_{2.5}$ mass concentration ranged from 5.0 μg m^{-3} to 143.8 μg m^{-3}, with an annual mean of 33.0 μg m^{-3} ± 20.0 μg m^{-3}, which was below the Grade I Chinese National Ambient Air Quality Standard (NAAS, 35 μg m^{-3}).

It can be seen from the mean seasonal $PM_{2.5}$ mass concentrations in Table 2 that the highest concentration was during the winter (13.0–102.4 μg m^{-3}, mean of 45.8 μg m^{-3} ± 20.5 μg m^{-3}), whereas the concentration during the summer were lowest (6.5–26.9 μg m^{-3}, mean of 20.8 μg m^{-3} ± 10.9 μg m^{-3}). This indicates that PM pollution still exist in the Guiyang urban atmosphere. The concentrations of WSIIs and TN were also highest during the winter. The mean annual

Table 2
Mean (and standard deviation) seasonal concentrations of $PM_{2.5}$ mass, ionic species, total particulate nitrogen (TN), and gaseous pollutants along with the mean ambient temperature and mean relative humidity measured in Guiyang from September 2017 to August 2018.

Component (unit)	Mean seasonal value and standard deviation				Annual value		
	Autumn	Winter	Spring	Summer	Min.	Max.	Mean
Cl^- (μg m^{-3})	0.2 ± 0.2	0.5 ± 0.3	0.2 ± 0.2	0.2 ± 1.1	0.0	10.1	0.3
NO_3^- (μg m^{-3})	2.9 ± 3.6	5.9 ± 4.2	2.2 ± 2.0	0.8 ± 0.5	0.4	20.0	3.0
SO_4^{2-} (μg m^{-3})	9.1 ± 4.9	10.3 ± 4.4	9.2 ± 4.2	5.8 ± 3.1	1.2	28.6	8.6
K^+ (μg m^{-3})	0.4 ± 0.2	0.8 ± 0.8	0.5 ± 0.4	0.3 ± 0.2	0.0	6.6	0.5
Na^+ (μg m^{-3})	0.1 ± 0.1	0.1 ± 0.2	0.1 ± 0.1		0.0	0.9	0.1
Ca^{2+} (μg m^{-3})	0.9 ± 2.1	3.2 ± 1.7	2.9 ± 1.3	2.1 ± 0.8	0.2	9.0	2.6
Mg^{2+} (μg m^{-3})	0.1	0.2 ± 0.1	0.1 ± 0.1	0.1	0.0	0.9	0.1
NH_4^+ (μg m^{-3})	2.2 ± 3.0	5.2 ± 2.4	3.5 ± 2.1	1.9 ± 1.2	0.1	13.7	3.4
TN (μg m^{-3})	3.2 ± 2.3	4.4 ± 3.2	1.1 ± 1.8	1.6 ± 0.6	0.5	15.9	3.5
WSIIs (μg m^{-3})	17.9 ± 10.8	26.3 ± 11	18.9 ± 8.1	11.1 ± 5.0	3.1	66.5	18.6
T (°C)	16.3 ± 5.61	5.8 ± 4.3	16.9 ± 4.4	23.0 ± 2.0	−3.3	26.3	15.5
RH (%)	79.4 ± 10.2	77.7 ± 15.1	76.0 ± 12.4	78 ± 9.9	9.9	100.0	77.7
CO (μg m^{-3})	0.7 ± 0.1	0.9 ± 0.2	0.7 ± 0.1	0.6 ± 0.1	0.1	1.5	0.7
NO_2 (μg m^{-3})	22.2 ± 9.8	30.5 ± 15.1	25.2 ± 10.3	20.9 ± 12.5	7.9	92.9	24.7
O_3 (μg m^{-3})	52.4 ± 21.9	53.4 ± 23.5	88.6 ± 23.5	81.1 ± 29.3	5.9	156.5	68.9
SO_2 (μg m^{-3})	10.9 ± 6.8	17.7 ± 8.6	8.8 ± 6.1	5.7 ± 4.9	1.4	45.0	10.8
$PM_{2.5}$ (μg m^{-3})	27.8 ± 19.5	45.8 ± 20.5	37.6 ± 18.1	20.8 ± 10.9	5.0	143.8	33.0
NOR	0.1 ± 0.1	0.2 ± 0.1	0.1 ± 0.1	0.1	0.1	0.5	0.1
$NH_4/(NO_3 + 2 \times SO_4)$	0.1 ± 0.7	0.9 ± 0.3	0.8 ± 0.4	0.8 ± 0.2	0.1	3.8	0.8

concentration of WSIIs was 18.6 μg m^{-3} ± 10.5 μg m^{-3}, which accounted for 56% for the total $PM_{2.5}$ mass. The TN concentration varied from 0.5 μg m^{-3} to 15.9 μg m^{-3} with an annual mean of 3.6 μg m^{-3} ± 2.7 μg m^{-3}, which accounted for 10.6% for the total $PM_{2.5}$ mass. The most predominant species of WSIIs was SO_4^{2-}, which accounted for 32.1% of the total WSII concentration, and was followed by NH_4^+ (17.6%), NO_3^- (13.1%), Ca^{2+} (15.8%), K^+ (2.6%), and Cl^- (1.3%). These results can be ascribed to a combination of influencing factors, including the atmospheric conditions (e.g., T, RH, and gaseous precursors; Fig. 3) and different sources.

3.2. Incremental increase of N species during the winter

The concentrations of the various WSIIs during each season are shown in Fig. 4a. As expected, the concentrations of all WSIIs increased considerably during the winter. The relative abundance of each WSII during each season is plotted in Fig. 4b. Although the SO_4^{2-} concentration increased during the winter, its relative abundance decreased from 52% during the summer to 22% during the winter. However, significant enhancements of the NO_3^- and NH_4^+ concentrations and relative abundances occurred during the winter, for example, the NO_3^- concentration increased by ~13% from the summer and winter. Both NO_3^- and NH_4^+ were dominant airborne N species, and exhibited a highest-to-lowest concentration ratio of 7.4 and 2.7, respectively, which were much higher than that of sulfate (1.8). A similar phenomenon was reported for Beijing, Shanghai, and Hangzhou, where NO_3^- and NH_4^+ concentrations increased more rapidly during the winter in comparison to the SO_4^{2-} concentration (Cheng et al., 2017; Pan et al., 2016; Tan et al., 2018; Wu et al., 2016). The significant enhancements of NO_3^- and NH_4^+ in the present study might be explained by more practical changes, for example, NH_3 (g) ↔ NH_4^+ (p) and HNO_3(g) ↔ NO_3^- (p) formation under a low ambient temperature condition.

In the atmosphere, NO_3^- mainly exists in the form of ammonium nitrate (NH_4NO_3). Several factors, including gaseous precursors, ambient temperature, and relative humidity, affect the formation and concentration of airborne particulate NO_3^-. For instance, NO_x is emitted from vehicles and stationary sources, and can undergo homogeneous (NO_2 + OH) and heterogeneous (N_2O_5 + H_2O) reactions to produce aqueous NO_3^-, which is neutralized by NH_4^+. Thus, NO_2 and NH_3, as precursors of NH_4NO_3, can influence the formation of particulate NH_4NO_3. On the other hand, the formation of particulate NH_4NO_3 is susceptible to the ambient RH and T (Lin and Cheng, 2007). A low T and high RH are favorable conditions for the yield of particulate NH_4NO_3. However, compared with the enhancements of NO_2 (1.5) during the winter, the increase of NO_3^- (7.4) in this study was much more remarkable (Table 2 and Fig. 4b). This result suggested that the high NO_3^- concentration during the winter was not only due to the T, but also to the increasing NO_x concentration and the atmospheric process of NO_3^- formation.

Nitrogen oxidation ratio (NOR) were used to evaluate the photochemical oxidation extent of NO_2. (Luo et al., 2019; Ohta and Okita, 1990; Sun et al., 2006) NOR are defined as the ratio of second species to total N, i.e. NOR = $nNO_3^-/(nNO_3^- + nNO_2)$, where n refers to molar concentration. Gas precursors NO_2 showed the same seasonal variations pattern as $PM_{2.5}$ and major ions (Table 2). It has been reported that when NOR exceeds 0.1, there is photochemical oxidation of NO_2 in the atmosphere.(Ohta and Okita, 1990) In this study, NOR was greater than 0.1 in four seasons, in addition. NOR was comparable among spring, summer, and autumn, while it was higher in Winter. This indicated that photochemical oxidation of NO_2 occurred all year round and was more efficient in Winter. The sudden increase of NO_3^- in winter could be explained as the low temperature promotes the oxidation efficiency of gaseous NO_2 (Lin and Cheng, 2007).

3.3. Seasonal variations in N concentrations and $\delta^{15}N$ signatures

The seasonal variations in TN concentration and $\delta^{15}N$ value during the study period are shown in Fig. 5. The TN concentration ranged from 0.5 μg m^{-3} to 15.9 μg m^{-3} (mean of 3.6 μg m^{-3} ± 2.7 μg m^{-3}), whereby the maximum and minimum TN concentrations were during the winter and spring, respectively. Seasonally, the $\delta^{15}N$ value of the TN exhibited the lowest values during the winter and highest values during the summer. This trend has also been observed in other studies undertaken in urban Paris, rural Brazil, Jeju Island, Baengnyeong Island, South Korea, and central Europe(Table 3) (Kundu et al., 2010; Martinelli

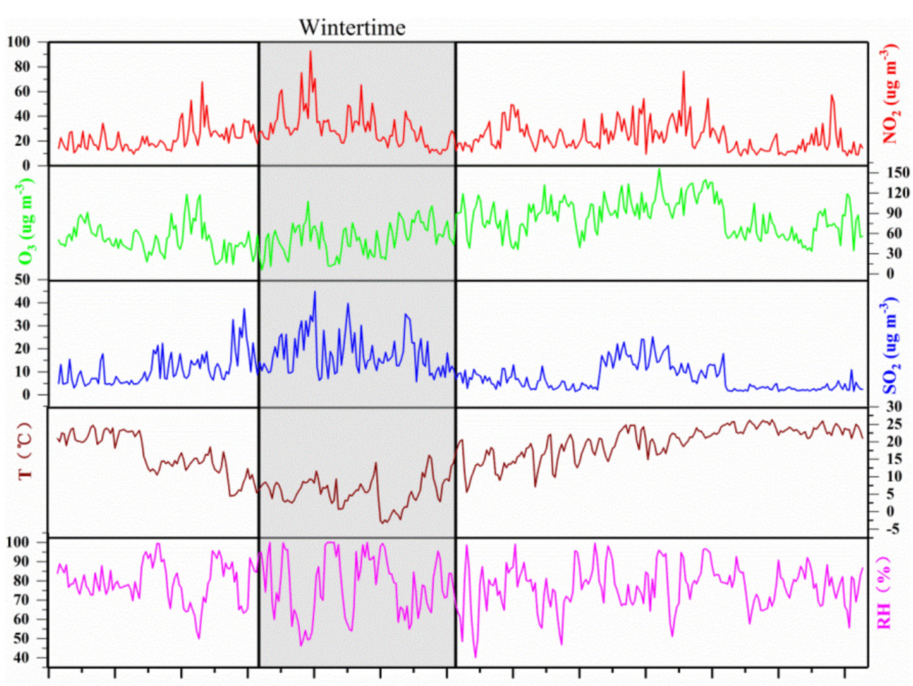

Fig. 3. Temporal variations of NO_2 (a), O_3 (b), and SO_2 (c) concentrations, and T (d) and RH (e) from September 2017 to August 2018. The shaded part represents wintertime.

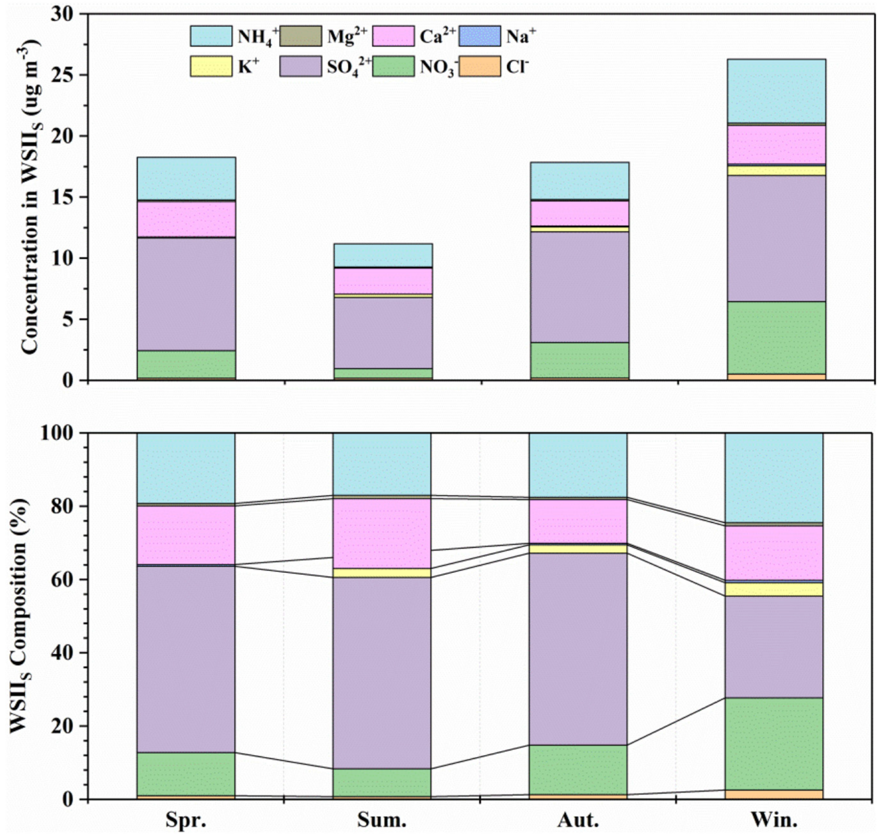

Fig. 4. Seasonal concentrations (a) and abundances (b) of ionic species in $PM_{2.5}$.

et al., 2002; Park et al., 2018; Vodicka et al., 2019; Widory, 2007). The $\delta^{15}N$ value was stable during the winter at approximately 7.0‰. There was a strong enrichment of ^{15}N during the summer in comparison to the winter, thus resulting in a mean value of 15.5‰. During the spring, we observed a slow increase in the $\delta^{15}N$ value from April to June, indicates a gradual change in the N chemistry in the atmosphere. The $\delta^{15}N$

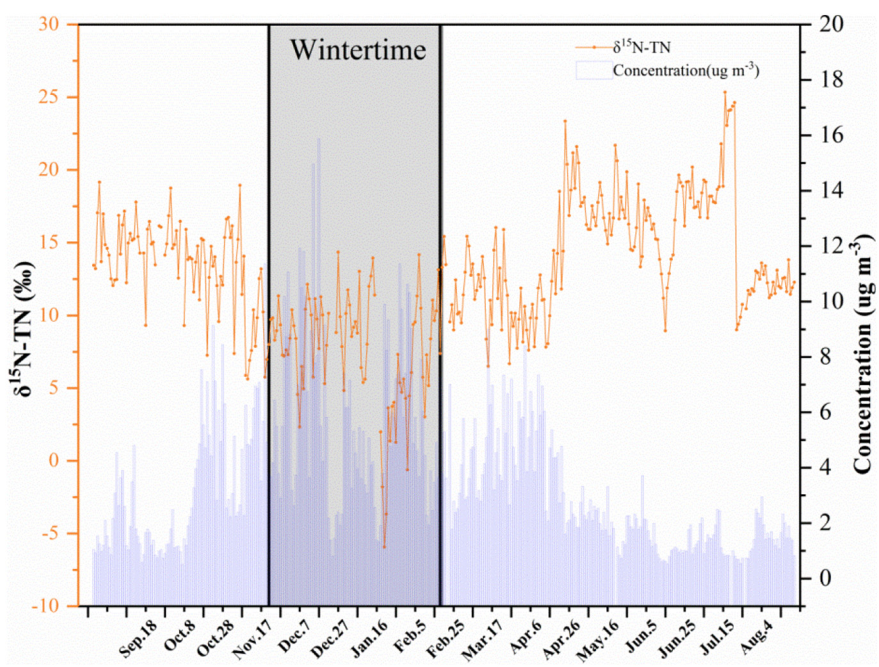

Fig. 5. Time series of the $\delta^{15}N$-TN value and TN concentration in $PM_{2.5}$ aerosols sampled in Guiyang. The gray color highlights winter data with different values, especially for $\delta^{15}N$. The shaded part represents the wintertime.

Table 3
Comparison of δ^{15}N-TN data from studies in various locations worldwide.

Location	Information	δ^{15}N-TN (‰)		Reference
		(Range)	Mean ± standard deviation	
Seoul (urban)	2014–2015; $PM_{2.5}$	4.3–18.9	12.4 ± 3.5	(Park et al., 2018)
Baengnyeong Island (rural)	2014–2015; $PM_{2.5}$	−8.1 to −18.9	3.9 ± 5.4	(Park et al., 2018)
IGP (urban)	01/2009; $PM_{2.5}$	11.8 to 30.6	20.4 ± 5.4	(Bikkina et al., 2016)
SEA (coastal)	01/2009; $PM_{2.5}$	10.4 to 31.7	19.4 ± 6.1	(Bikkina et al., 2016)
Dai Ang Kang	3/1/2015–4/13/2015; $PM_{2.5}$	15.8–25.1	19.4 ± 2.1	(Boreddy et al., 2018)
Gosan, Kore (rural)	2003; $PM_{2.5}$	6.8–26.9	15.1 ± 3.4	(Kundu et al., 2010)
Central Europe (rural)	2013; PM_1	13.1–25	17.8 ± 5.5	(Vodicka et al., 2019)
Guiyang, China (urban)	2017–2018; $PM_{2.5}$	−5.9 to 25.3	11.8 ± 4.7	This study

value ranged widely from −5.9‰ to 25.3‰ over the year of sampling, possibly due to the complexity of N-containing species or components in aerosols.

3.4. Source apportionment of TN in $PM_{2.5}$ during the winter

According to the source appointment method of aerosol Nat Guiyang (Zhao et al., 2019), the following seven dominant sources can be assigned for the total N of $PM_{2.5}$.

S1: NO_2 from coal combustion;
S2: NO_2 from vehicle exhausts;
S3: NO_2 from biomass burning;
S4: NH_3 from coal combustion;
S5: NH_3 from vehicle exhausts;
S6: NH_3 from biomass burning;
S7: NH_3 from animal waste (mainly domestic waste and sewages).

We note that although NO is the initial precursor of NO_2 emission sources, it is quite reactive and readily oxidized to NO_2, which is more often regarded as the precursor of NO_3^- in the atmosphere. Thus, NO_2 was used in this work uniformly, and its δ^{15}N values were assumed as those of the corresponding NO_x emissions.

In this study, agricultural and biogenic N-emissions were not considered as significant sources of TN in $PM_{2.5}$ in Guiyang for two main reasons. First, the sampling site was located in the urban center of Guiyang. Several studies have shown that N deposition is mainly influenced by anthropogenic sources (Liu et al., 2017; Zhao et al., 2019). Second, during the winter, the contributions of NO_2 from the microbial N-cycle, NH_3 emissions from seawater ($\delta^{15}N = -8$‰ to −5‰), and lightning NO_x ($\delta^{15}N = -0.5$‰ to +1.4‰) to the formation of near-surface $PM_{2.5}$ are relatively lower than the contributions from anthropogenic N-sources, especially in urban areas (Hoering, 1960).

To date, the δ^{15}N values of various NO_2 and NH_3 emissions have been unavailable in China. However, according to source δ^{15}N data compiled from previous studies (Table 1),.in which isotopic tracing or partitioning of atmospheric N have been used.(Elliott et al., 2009; Kawashima and Kurahashi, 2011) To quantitatively estimate the source apportionments of airborne TN, seven dominant N-sources served as input data to the SIAR model. Table1 lists the δ^{15}N-NO_x and δ^{15}N-NH_3 values for our selected sources.

In the calculations, the actual molar concentration of $NH_4{}^+$ in $PM_{2.5}$ was used, while the ($NO_3^- + 2 \times SO_4^{2-}$) in $PM_{2.5}$ represents the $NH_4{}^+$concentration that can be fixed by NO_3^- and SO_4^{2-}. The molar ratio of $NH_4^+/(NO_3^- + 2 \times SO_4^{2-})$ during the winter calculated as 0.9 (Table 2), thus indicating that NO_3^- and SO_4^{2-} in $PM_{2.5}$ in Guiyang completely fixed NH_4^+. Thus, no substantial ^{15}N enrichment of NH_4^+ in $PM_{2.5}$ was observed(Kawashima and Kurahashi, 2011; Pavuluri et al., 2010; Yeatman et al., 2001b). Consequently, the δ^{15}N values of $PM_{2.5}$ in Guiyang were assumed to have been mainly controlled by mixed N-sources, since there's no extra NH_4^+ plus, continuously process of NH_4^+ (p)— > NH_3 (g) would not happen, with an inappreciable effect of isotopic fractionation and no substantial isotopic effect between N sources.

The estimated contributions of the potential N-sources to the TN of $PM_{2.5}$ during the winter in Guiyang are shown in Fig. 6. As illustrated, potential NH_3 (PNH_3) emissions contributed 49% of the total TN of $PM_{2.5}$, while potential NOx (PNO_x) emissions contributed 51% during the winter. The mean ratio of PNH_3 to PNO_x was 0.96. According to the estimations, NH_3 from combustion-related sources contributed 39% to TN of $PM_{2.5}$, which was the most predominant source and was followed by NO_x derived from fossil fuels (32%), NH_3 from animal waste (9%), and NO_x and NH_3 from biomass burning (20%). As a result, biomass burning was the main contributor during the winter. The influence of the changes could be explained by the 72 h air-mass backward trajectories, which shows obvious seasonal differences. During the winter, 41% of the air mass comes from the Guizhou/Chongqing border, 39% from the Guizhou/Guangxi border, 11% from north China, and 9% from northwest India. Eighty percent of the air mass comes from rural areas, where people still have the habit of burning wood for warming and cooking in winter. A limitation of this research was that we did not consider the influence of ON (organic nitrogen), such that the results are associated with some uncertainty; hence, we will take this into account in our future work.

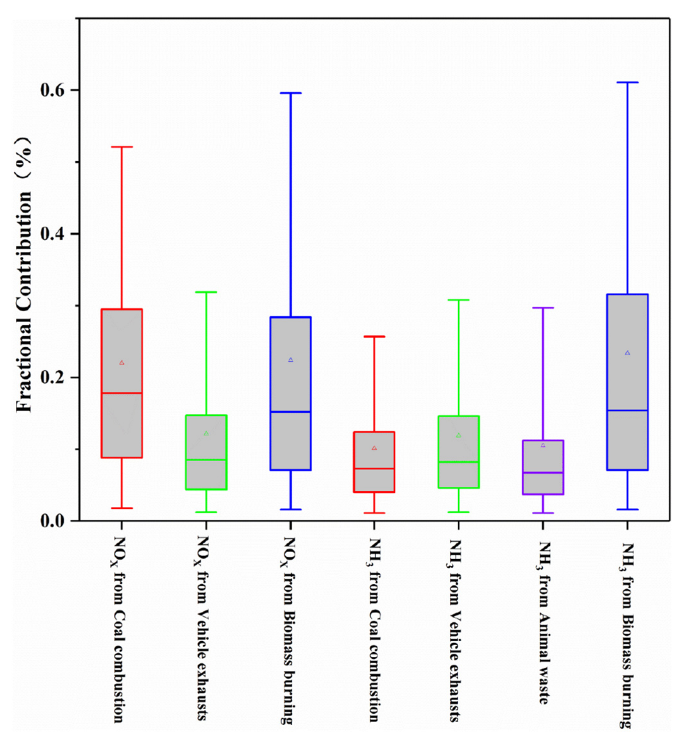

Fig. 6. Relative contributions of potential nitrogen sources to airborne $PM_{2.5}$ TN in Guiyang during the winter. The box encompasses the 25th–75th percentiles, and the whiskers are the 10th and 90th percentiles. The lines inside the boxes indicate the median values and the triangles represent to mean values.

4. Conclusion

To comprehend the trend and source apportionment, we investigated WSIIs and the $\delta^{15}N$ value of TN in $PM_{2.5}$ in Guiyang from September 2017 to August 2018. The main conclusions from this work are as follows. The $PM_{2.5}$ concentration ranged from 5.0 μg m^{-3} to 143.8 μg m^{-3} (mean value of 33.0 μg m^{-3} ± 20 μg m^{-3}). Water-soluble inorganic ions accounted for 56% of the $PM_{2.5}$ mass, with SO_4^{2-} being the most predominant species, followed by NH_4^+ and NO_3^-. The TN species in $PM_{2.5}$ were mainly NH_4^+-N and NO_3^--N constituting a total of 11% of $PM_{2.5}$. Compared to the concentrations during other seasons, all species exhibited high concentrations during the winter, especially NO_3^-. These valuable data provide an indication of the potential sources of particulate TN. The results showed that the $\delta^{15}N$ value in TN varied from −5.9‰ to +13.2‰ (mean value of 7.0‰ ± 3.6‰) during the winter. This finding was coupled to the SIAR model and $\delta^{15}N$ values to indicate the potential sources of TN in $PM_{2.5}$. We suggest that controlling the N-emissions from wintertime biomass burning in the rural area of Guizhou border might be a useful way to improve the air quality during the winter. This study used a relatively straightforward approach for quantifying the sources of N-containing aerosols, and there were considerable uncertainties due to the complex fractionation of $\delta^{15}N$ during chemical conversions (i.e., $NO_x(NH_3)$ to $NO_3^-(NH_4^+)$). Moreover, we did not adequately consider isotope fractionation in the source measurements, which was partly due to the minimal knowledge that exists regarding in-situ fractionation mechanisms. The $\delta^{15}N$ value of different species in aerosols would be will better explain the nitrogen production of the secondary aerosol in the atmosphere, and better understand the variation and origin of N-species in the atmosphere.

CRediT authorship contribution statement

Jing Tian: Methodology, Data curation, Writing – original draft. **Hui Guan:** Methodology, Supervision, Writing – review & editing. **Zhongyi Zhang:** Data curation, Investigation. **Nengjian Zheng:** Data curation, Investigation. **Hongwei Xiao:** Data curation, Investigation. **Jingjing Zhao:** Investigation, Visualization. **Yunhong Zhou:** Investigation, Visualization. **Huayun Xiao:** Conceptualization, Methodology, Supervision, Writing – review & editing.

Declaration of competing interest

The authors declare that they have no known competing financial interests or personal relationships that could have appeared to influence the work reported in this paper.

Acknowledgments

This study was kindly supported by the National Natural Science Foundation of China through grant number 41425014.

References

Bikkina, S., Kawamura, K., Sarin, M., 2016. Stable carbon and nitrogen isotopic composition of fine mode aerosols (PM2.5) over the Bay of Bengal: impact of continental sources. Tellus B: Chemical and Physical Meteorology 68, 31518.

Boreddy, S.K.R., Parvin, F., Kawamura, K., Zhu, C., Lee, C., 2018. Stable carbon and nitrogen isotopic compositions of fine aerosols (PM2.5) during an intensive biomass burning over Southeast Asia: Influence of SOA and aging. Atmos. Environ. 191, 478–489.

Cheng, C., Ganganath, N., Fok, K., 2017. Concurrent data collection trees for IoT applications. IEEE Transactions on Industrial Informatics 13, 793–799.

Elliott, E.M., Kendall, C., Boyer, E.W., Burns, D.A., Lear, G.G., Golden, H.E., et al., 2009. Dual nitrate isotopes in dry deposition: utility for partitioning NOx source contributions to landscape nitrogen deposition. Journal of Geophysical Research-Biogeosciences 114.

Evans, J.S.B.T., Handley, S.J., Perham, N., Over, D.E., Thompson, V.A., 2000. Frequency versus probability formats in statistical word problems. Cognition 77, 197–213.

Felix, J.D., Elliott, E.M., Gish, T.J., Maghirang, R., Cambal, L., Clougherty, J., 2014. Examining the transport of ammonia emissions across landscapes using nitrogen isotope ratios. Atmos. Environ. 95, 563–570.

Felix, J.D., Elliott, E.M., Gish, T.J., McConnell, L.L., Shaw, S.L., 2013. Characterizing the isotopic composition of atmospheric ammonia emission sources using passive samplers and a combined oxidation-bacterial denitrifier approach. Rapid Commun. Mass Spectrom 27, 2239–2246.

Felix, J.D., Elliott, E.M., Shaw, S.L., 2012. Nitrogen isotopic composition of coal-fired power plant NOx: influence of emission controls and implications for global emission inventories. Environ. Sci. Technol 46, 3528–3535.

Freyer, H.D, 1978. Preliminary 15N studies on atmospheric nitrogenous trace gases. Pure Appl. Geophys 116(2-3), 393–404.

Fuzzi, S., Baltensperger, U., Carslaw, K., Decesari, S., Denier van der Gon, H., Facchini, M.C., et al., 2015. Particulate matter, air quality and climate: lessons learned and future needs. Atmos. Chem. Phys. 15, 8217–8299.

Hastings, M.G., Jarvis, J.C., Steig, E.J., 2009. Anthropogenic impacts on nitrogen isotopes of ice-core nitrate. Science 324, 1288.

He, P., Xie, Z., Chi, X., Yu, X., Fan, S., Kang, H., et al., 2018. Atmospheric $\delta^{17}O(NO_3^-)$ reveals nocturnal chemistry dominates nitrate production in Beijing haze. Atmos. Chem. Phys. 18, 14465–14476.

He, P., Xie, Z., Yu, X., Wang, L., Kang, H., Yue, F., 2020. The observation of isotopic compositions of atmospheric nitrate in Shanghai China and its implication for reactive nitrogen chemistry. Sci. Total Environ. 714, 136727.

Heaton, T.H.E., 1986. Isotope studies of nitrogen pollution in the hydrosphere and atmosphere-a review. Chem. Geol. 59, 87–102.

Heaton, T.H.E., 1987. 15N/14N ratios of nitrate and ammonium in rain at Pretoria, South Africa. Atmos. Environ 21(4), 843–852.

Hegde, P., Kawamura, K., Joshi, H., Naja, M., 2016. Organic and inorganic components of aerosols over the central Himalayas: winter and summer variations in stable carbon and nitrogen isotopic composition. Environ. Sci. Pollut. Res. 23, 6102–6118.

Hoering, Thomas, 1960. The isotopic composition of the ammonia and the nitrate ion in rain. Geochim. Cosmochim. Acta 12, 97–102.

Jackson, A.L., Inger, R., Bearhop, S., Parnell, A., 2009. Erroneous behaviour of MixSIR, a recently published Bayesian isotope mixing model: a discussion of Moore & Semmens (2008). Ecol. Lett. 12, E1–E5.

Jiang, Y., Zhuang, G., Wang, Q., Huang, K., Deng, C., Yu, G., et al., 2018. Impact of mixed anthropogenic and natural emissions on air quality and eco-environment—the major water-soluble components in aerosols from northwest to offshore isle. Air Quality, Atmosphere & Health 11, 521–534.

Kawashima, H., Kurahashi, T., 2011. Inorganic ion and nitrogen isotopic compositions of atmospheric aerosols at Yurihonjo, Japan: implications for nitrogen sources. Atmos. Environ. 45, 6309–6316.

Kendall, C., Elliott, E., Wankel, S., 2008. Tracing Anthropogenic Inputs of Nitrogen to Ecosystems. pp. 375–449.

Kundu, S., Kawamura, K., Lee, M., 2010. Seasonal variation of the concentrations of nitrogenous species and their nitrogen isotopic ratios in aerosols at Gosan, Jeju Island: implications for atmospheric processing and source changes of aerosols. J. Geophys. Res. 115.

Li, Y.J., Sun, Y., Zhang, Q., Li, X., Li, M., Zhou, Z., et al., 2017. Real-time chemical characterization of atmospheric particulate matter in China: a review. Atmos. Environ. 158, 270–304.

Liang, L., Engling, G., Zhang, X., Sun, J., Zhang, Y., Xu, W., et al., 2017. Chemical characteristics of PM2.5 during summer at a background site of the Yangtze River Delta in China. Atmos. Res. 198, 163–172.

Lin, Y.C., Cheng, M.T., 2007. Evaluation of formation rates of NO_2 to gaseous and particulate nitrate in the urban atmosphere. Atmos. Environ. 41, 1903–1910.

Liu, X.-Y., Xiao, H.-W., Xiao, H.-Y., Song, W., Sun, X.-C., Zheng, X.-D., et al., 2017. Stable isotope analyses of precipitation nitrogen sources in Guiyang, southwestern China. Environ. Pollut. 230, 486–494.

Luo, L., Wu, Y., Xiao, H., Zhang, R., Lin, H., Zhang, X., et al., 2019. Origins of aerosol nitrate in Beijing during late winter through spring. Science of The Total Environment 653, 776–782.

Martinelli, L.A., Camargo, P.B., Lara, L., Victoria, R.L., Artaxo, P., 2002. Stable carbon and nitrogen isotopic composition of bulk aerosol particles in a C4 plant landscape of southeast Brazil. Atmos. Environ. 36, 2427–2432.

Michalski, G., Meixner, T., Fenn, M., Hernandez, L., Sirulnik, A., Allen, E., et al., 2004. Tracing atmospheric nitrate deposition in a complex semiarid ecosystem using Δ17O. Environmental Science & Technology 38, 2175–2181.

Moore, J.W., Semmens, B.X., 2008. Incorporating uncertainty and prior information into stable isotope mixing models. Ecol. Lett. 11, 470–480.

Ohta, S., Okita, T., 1990. A chemical characterization of atmospheric aerosol in Sapporo. Atmos. Environ. Part A 24A, 815–822.

Pan, Y., Wang, Y., Zhang, J., Liu, Z., Wang, L., Tian, S., et al., 2016. Redefining the importance of nitrate during haze pollution to help optimize an emission control strategy. Atmos. Environ. 141, 197–202.

Park, Y.-m., Park, K.-s., Kim, H., Yu, S.-m., Noh, S., Kim, M.-s., et al., 2018. Characterizing isotopic compositions of TC-C, $NO_3(-)$-N, and NH^{4+}-N in PM2.5 in South Korea: impact of China's winter heating. Environ. Pollut. 233, 735–744.

Parnell, A.C., Inger, R., Bearhop, S., Jackson, A.L., 2010. Source partitioning using stable isotopes: coping with too much variation. PLoS One 5.

Pavuluri, C.M., Kawamura, K., Tachibana, E., Swaminathan, T., 2010. Elevated nitrogen isotope ratios of tropical Indian aerosols from Chennai: implication for the origins of aerosol nitrogen in South and Southeast Asia. Atmos. Environ. 44, 3597–3604.

Petäjä, T., Järvi, L., Kerminen, V.M., Ding, A.J., Kulmala, M., 2016. Enhanced Air Pollution via Aerosol-boundary Layer Feedback in China.

Pope, C.A.I., Majid, E., Douglas, W., 2009. D. Fine-particulate air pollution and life expectancy in the United States. New England Journal of Medicine 360, 376.

Savarino, J., Morin, S., Erbland, J., Grannec, F., Patey, M.D., Vicars, W., et al., 2013. Isotopic composition of atmospheric nitrate in a tropical marine boundary layer. Proc. Natl. Acad. Sci. U. S. A. 110, 17668–17673.

Sun, Y., Zhuang, G., Tang, A., Wang, Y., An, Z., 2006. Chemical characteristics of PM2.5 and PM10 in haze-fog episodes in Beijing. Environmental Science & Technology 40, 3148–3155.

Tan, T., Hu, M., Li, M., Guo, Q., Wu, Y., Fang, X., et al., 2018. New insight into PM2.5 pollution patterns in Beijing based on one-year measurement of chemical compositions. Sci. Total Environ. 621, 734–743.

Tao, J., Zhang, Z., Tan, H., Zhang, L., Wu, Y., Sun, J., et al., 2018. Observational evidence of cloud processes contributing to daytime elevated nitrate in an urban atmosphere. Atmos. Environ. 186, 209–215.

Vodicka, P., Kawamura, K., Schwarz, J., Kunwar, B., Zdimal, V., 2019. Seasonal study of stable carbon and nitrogen isotopic composition in fine aerosols at a Central European rural background station. Atmos. Chem. Phys. 19, 3463–3479.

Wang Y-L, Liu X-Y, Song W, Yang W, Han B, Dou X-Y, et al. Source appointment of nitrogen in PM2.5 based on bulk δ15N signatures and a Bayesian isotope mixing model. Tellus Series B-chemical & Physical Meteorology.

Walters, Wendell W., Goodwin, Stanford.R, Michalski, Greg, 2015. The Nitrogen Stable Isotope Composition (δ15N) of Vehicle Emitted NOx. Environ. Sci. Technol 49, 2278–2285.

WHO, 2018. 9 out of 10 People Worldwide Breathe Polluted Air, but More Countries Are Taking Action.

Widory, D., 2007. Nitrogen isotopes: tracers of origin and processes affecting PM in the atmosphere of Paris. Atmos. Environ. 41, 2382–2390.

Wu, J., Xu, C., Wang, Q., Cheng, W., 2016. Potential sources and formations of the PM2.5 pollution in urban Hangzhou. Atmosphere 7.

Xiao, H.Y., Liu, C.Q., 2002. Sources of nitrogen and sulfur in wet deposition at Guiyang, southwest China. Atmos. Environ. 36, 5121–5130.

Xu, J.-S., Xu, M.-X., Snape, C., He, J., Behera, S.N., Xu, H.-H., et al., 2017a. Temporal and spatial variation in major ion chemistry and source identification of secondary inorganic aerosols in Northern Zhejiang Province, China. Chemosphere 179, 316–330.

Xu, L., Duan, F., He, K., Ma, Y., Zhu, L., Zheng, Y., et al., 2017b. Characteristics of the secondary water-soluble ions in a typical autumn haze in Beijing. Environ. Pollut. 227, 296–305.

Xu, Y., Xiao, H., Qu, L., 2017c. Nitrogen concentrations and nitrogen isotopic compositions in leaves of Cinnamomum Camphora and Pinus massoniana (Lamb.) for indicating atmospheric nitrogen deposition in Guiyang (SW China). Atmos. Environ. 159, 1–10.

Yeatman, S.G., Spokes, L.J., Dennis, P.F., Jickells, T.D., 2001a. Can the study of nitrogen isotopic composition in size-segregated aerosol nitrate and ammonium be used to investigate atmospheric processing mechanisms? Atmos. Environ. 35, 1337–1345.

Yeatman, S.G., Spokes, L.J., Jickells, T.D., 2001b. Comparisons of coarse-mode aerosol nitrate and ammonium at two polluted coastal sites. Atmos. Environ. 35, 1321–1335.

Zhang, Q., Ma, X., Tie, X., Huang, M., Zhao, C., 2009. Vertical distributions of aerosols under different weather conditions: analysis of in-situ aircraft measurements in Beijing, China. Atmos. Environ. 43, 5526–5535.

Zhang, Z, Guan, H, Luo, L, et al., 2020a. Sources and transformation of nitrate aerosol in winter 2017–2018 of megacity Beijing: Insights from an alternative approach. Atmos. Environ. 241, 117842.

Zhang, Z, Zheng, N, Zhang, D, 2020b. Rayleigh based concept to track NOx emission sources in urban areas of China. Sci. Total. Environ. 704, 135362.

Zhang, Z, Zeng, Y, Zheng, N, 2020c. Fossil fuel-related emissions were the major source of NH3 pollution in urban cities of northern China in the autumn of 2017. Environ. Pollut. 256, 113428.

Zhao, J., Zhang, Z., Zhu, G., Zheng, N., Xiao, H., Tian, J., et al., 2019. The δ15N values of epilithic mosses indicating the changes of nitrogen sources in Guiyang (SW China) from 2006 to 2016–2017. Sci. Total Environ. 696, 133988.